Contract No:

This document was prepared in conjunction with work accomplished under Contract No. DE-AC09-08SR22470 with the U.S. Department of Energy.

Disclaimer:

SRNL-STI-2008-00541

Hierarchical Methodology for Modeling Hydrogen Storage Systems. Part II: Detailed Models

Bruce J. Hardy*, Donald L. Anton
Savannah River National Laboratory, Aiken, SC 29808 USA

ABSTRACT

There is significant interest in hydrogen storage systems that employ a media which either adsorbs, absorbs or reacts with hydrogen in a nearly reversible manner. In any media based storage system the rate of hydrogen uptake and the system capacity is governed by a number of complex, coupled physical processes. To design and evaluate such storage systems, a comprehensive methodology was developed, consisting of a hierarchical sequence of models that range from scoping calculations to numerical models that couple reaction kinetics with heat and mass transfer for both the hydrogen charging and discharging phases. The scoping models were presented in Part I [1] of this two part series of papers. This paper describes a detailed numerical model that integrates the phenomena occurring when hydrogen is charged and discharged. A specific application of the methodology is made to a system using $NaAlH_4$ as the storage media.

Keywords: Hydrogen Storage Modeling, Hydrogen Storage Systems, Metal Hydrides, Hierarchical Modeling System

* Corresponding author. Tel.: (803) 725-7310; Fax: (803) 725-8829;
E-mail address: bruce.hardy@srnl.doe.gov

NOMENCLATURE

C = Concentration of H_2 in the bed void space [mole H_2/m^3]

C_{eqv} = Equivalent concentration of $NaAlH_4$ [mole/m^3] based on the initial concentrations of all metal species

= $C_{10} + 3C_{20} + C_{30}$

C_{NaH} = Bulk concentration of NaH [mole NaH/m^3]

C_{NaAlH_4} = Bulk concentration of $NaAlH_4$ [mole $NaAlH_4/m^3$]

C_{nd} = The non-dimensionalized concentration of H_2 = $\frac{C}{C_{ref}}$

$C_{p\ H_2}$ = Specific heat of H_2 [J/(kg-K)]

$C_{p_{metal}}$ = Specific heat of the metal [J/(kg-K)]

C_{ref} = Reference H_2 concentration in the bed void space [mole/m^3]

C_1 = Bulk concentration of $NaAlH_4$ [mole/m^3]

C_2 = Bulk concentration of Na_3AlH_6 [mole/m^3]

C_3 = Bulk concentration of NaH [mole/m^3]

$C_{1\,0}$ = Initial bulk concentration of $NaAlH_4$ [mole/m^3]

$C_{2\,0}$ = Initial bulk concentration of Na_3AlH_6 [mole/m^3]

$C_{3\,0}$ = Initial bulk concentration of NaH [mole/m^3]

D_p = Mean diameter of particles in bed [m]

$h_{conv\ cool}$ = Convection heat transfer coefficient for heat transfer fluid [W/m^2-°C]

$h_{H_2\ cool}$ = Convection heat transfer coefficient for H_2 in the feed tube [W/m^2-°C]

k = Bed thermal conductivity [W/(m-K)]

k_{metal} = Thermal conductivity of the metal [W/(m-K)]

M_{H_2} = Molecular weight of H_2 [kg/g-mole]

M_{NaH} = Molecular weight of NaH [kg/g-mole]

M_{NaAlH_4} = Molecular weight of $NaAlH_4$ [kg/g-mole]

$M_{Na_3AlH_6}$ = Molecular weight of Na_3AlH_6 [kg/g-mole]

$\hat{n}$ = Outward normal to surface

P = Pressure [Pa]

P_{inj} = H_2 pressure in the feed tube [Pa]

P_{nd} = $\frac{P}{P_{ref}}$ =Non-dimensional pressure

$P_{eq1}(T)$ = H_2 pressures in equilibrium at temperature, T, with the $NaAlH_4$ [Pa]

$P_{eq2}(T)$ = H_2 pressures in equilibrium at temperature, T, with the Na_3AlH_6 [Pa]

P_{ref} = Reference pressure [Pa]

R = Gas constant = 8.314 J/(mol K)

S_{H_2} = Rate of H_2 generation per volume of bed from all chemical reactions

[mol H_2/(m^3 s)],

$S_{H_2} > 0$ if H_2 is produced

$S_{H_2} < 0$ if H_2 is removed

Source = Enthalpy change due to chemical reactions [W/m^3]

t = Time [s]

T = Temperature [K]

$T_{coolant\ bulk}$ = Bulk temperature of the heat transfer fluid [K]

$T_{nd} = \frac{T}{T_{ref}}$ = Non-dimensional temperature

$T_{H_2\ bulk}$ = Bulk temperature of the H_2 in the feed tube [K]

T_{ref} = Reference temperature [K]

T_{wall} = Tube wall temperature [K]

$\vec{v}$ = Mean interstitial H_2 velocity [m/s]

u = x component of the mean interstitial velocity, $\vec{v}$ [m/s]

$u_{nd} = \frac{u}{U_{ref}}$ = Non-dimensional x-component of the mean interstitial velocity

U_{ref} = Reference velocity [m/s]

v = y component of the mean interstitial velocity, $\vec{v}$ [m/s]

$v_{nd} = \frac{v}{U_{ref}}$ = Non-dimensional y-component of the mean interstitial velocity

w = z component of the mean interstitial velocity, $\vec{v}$ [m/s]

$w_{nd} = \frac{w}{U_{ref}}$ = Non-dimensional z-component of the mean interstitial velocity

Greek

ΔH_i = Enthalpy of reaction on a molar basis of species i [J/(mole of i)]

$\Delta H_{rxn\ 1}$ = Heat of reaction per mole of H_2 consumed going to left for reaction 1

$\Delta H_{rxn\ 2}$ = Heat of reaction per mole of H_2 consumed going to left for reaction 2

ε = Void fraction (porosity) of particle bed

μ = Viscosity of H_2 [Pa-s]

$\left.\frac{\nu_{H_2}}{\nu_{NaH}}\right|_{Rxn2}$ = Ratio of the stoichiometric coefficient of H_2 to NaH in reaction 2

of Eq. 2 = 0.5

$\left.\frac{\nu_{H_2}}{\nu_{NaAlH_4}}\right|_{Rxn1}$ = Ratio of the stoichiometric coefficient of H_2 to $NaAlH_4$ in reaction 1

of Eq. 2 = 1

ρ = Mass density [kg/m^3]

ρ_{bed} = Bulk mass density of bed [kg/m^3] = $(1-\varepsilon)\rho_{bed\_particle}$ = $\frac{\text{Mass of solid}}{\text{Total volume}}$

$\rho_{bed\_particle}$ = Particle mass density of bed [kg/m^3] = $\frac{\text{Mass of solid}}{\text{Volume of solid}}$

$\rho_{bed} C_{p\ bed}$ = $\rho_{Solid\ Reactants} C_{p\ Solid\ Reactants} + \rho_{Solid\ Products} C_{p\ Solid\ Products}$

ρ_{H_2} = Hydrogen density [kg/m^3]

ρ_i = Bulk mass density of species i [kg/m^3]

ρ_{metal} = Density of the metal [kg/m^3].

Symbols and Operators

∇ = Gradient [1/m].

INTRODUCTION

It is difficult and expensive to design and conduct experiments that fully measure the complex processes occurring during the loading and discharge of hydrogen from a storage media, let alone perform sensitivity studies for a complete system. Any such experiments would be limited to a particular hydride and system design. Without a great deal of experience it is very difficult to know, a priori, the type and location of necessary measurements required to characterize the performance of the system.

A much more efficient approach is to evaluate proposed designs for hydrogen storage systems through the use of numerical models that couple heat and mass transport with the reaction kinetics occurring in the bed. By systematically combining scoping models that quickly evaluate whether a storage system has the potential to meet performance targets with more sophisticated models that provide detailed predictions of operational performance, the most promising designs can be efficiently identified. The modeling hierarchy presented in [1] and in this paper uses scoping models to screen out designs that perform poorly relative to target criteria and to provide input to detailed models,

which require more effort to apply. The detailed models are applied to viable system designs to provide an accurate evaluation of system performance, conduct sensitivity studies and to identify design improvements. Those systems that best approach the performance criteria may then be tested as prototypes, greatly reducing the number of necessary experiments. Required measurements, and locations at which they should be taken, would be identified from the detailed models.

In the past, a number of numerical models have been developed for metal hydride beds, [2-32]. A detailed survey of prior work is presented in Hardy [33]. These models have attempted to address, at least in part, the phenomena occurring as the bed is charged with or discharges hydrogen. The models, however, tended to be either of limited scope, were applied over a narrow range of operating conditions or lacked the flexibility to accommodate significant design modifications. Moreover, work in these references focused on predicting the behavior of particular design concepts rather than developing a systematic, quantitative methodology for identifying and analyzing storage system designs (storage vessel and media combinations) that satisfied practical performance criteria.

Scoping models for charging/discharging reaction kinetics, determination of system length scales and identification of heat removal parameters for storage systems and associated media were discussed in Hardy and Anton [1]. This paper, Part 2 of a two part series, is based on Hardy [33], and describes a detailed numerical model for hydrogen

storage systems. The detailed model, developed using the COMSOL Multiphysics®, version 3.3.0.405, finite element software [34], couples reaction kinetics with heat and mass transfer, for both charging and discharging of the storage media. In its 2-dimensional form the detailed model serves to provide rapid evaluation of bed configurations and physical processes. The 3-dimensional form of the model, which requires a considerably longer time to run, is used to investigate effects that do not readily lend themselves to 2-dimensional representations.

MODEL APPLICATION

Geometry and Storage Media

Although it is general and can be adapted to any geometry or storage media, the detailed 2 and 3-dimensional finite element models are applied to a storage system utilizing $TiCl_3$ catalyzed $NaAlH_4$, as were the Scoping Models in Hardy and Anton [1]. Although this media was shown to fall short of the 2010 U.S. Department of Energy (DOE) technical targets given in Attachment 3 of [33], it was used in the application because:

1. To the author's knowledge, it was the only complex metal hydride having sufficient chemical kinetics data for an engineering model of the recharging process.
2. The kinetics equations posed a significant challenge for this demonstration of the detailed model.

The storage system has the configuration of a cylindrical shell, tube and fin heat exchanger. The bed is divided by an array of fins that are normal to the axis and extend in the radial direction. The fins are press-fit to coolant tubes that are parallel to the axis. The left illustration in Figure 1 shows a storage system developed and tested by the United Technologies Research Center™ (UTRC™), see Mosher, et al. [31], which has a similar geometric configuration to the system modeled in this document.

Specifically, the detailed models were applied to a storage system having 9 coolant tubes and 8 tubes used to inject hydrogen into the hydride bed, see the right illustration in Figure 1. The model focuses on a layer of hydride material located at sufficient distance from the axial ends of the bed that the axial boundary conditions are periodic from the axial midplane of one fin to the axial midplane of the adjacent fin. Therefore, axial symmetry conditions can be applied to the axial midplane of the hydride layer and the axial midplane of the fin. Further, there are planes of azimuthal symmetry, as shown in the right illustration in Figure 1. The geometry used for the 3-dimensional model, along with the mesh, is shown in Figure 2. The geometry for the 2-dimensional model is a planar representation of this geometry.

The application the detailed model to the UTRC™ sodium alanate based modified shell, tube and fin heat exchanger represents:

1. A demonstration of the capabilities of the detailed model.
2. The first 3-dimensional model of this storage system.

3. The first application of a model that couples mass, momentum and energy transport with chemical kinetics for this storage system.

Model Assumptions

Assumptions made in the model are:

1 Only hydrogen is allowed to flow in the system.

2 The media bed does not expand or contract. This assumption is especially significant as media proposed for hydrogen storage experiences expansion or contraction during hydrogen charging and discharging, respectively.

3 The thermal properties of the bed do not change with the amount of hydrogen loading.

4 The thermal properties of the bed do not vary with temperature.

5 The characteristics of the bed are unaffected by the number of loading-unloading cycles. That is, aging/cycling of the media is neglected.

6 Heat transfer from the bed occurs via the heat transfer fluid (in the cooling tubes), by convection to the hydrogen in the feed tubes, and by homogeneous heat exchange with hydrogen flowing through the bed.

7 The solid material and hydrogen have the same instantaneous temperature at all locations within the bed.

8 The thermal conductivity, specific heat and viscosity of hydrogen do not vary with pressure over the operational regime of the storage system.

9 The tubes and fins are composed of 6063 T83 aluminum.

10 Thermal contact between the bed and the cooling tubes, the bed and the fin, and the fin and the cooling tubes is good, i.e. thermal contact resistance is neglected.

11 The bed void fraction remains constant and uniform throughout.

12 The bed fills the entire volume of the space between the fins and tubes.

13 The bulk temperature of the heat exchange fluid and the hydrogen supplied to the bed is constant and uniform.

14 The hydrogen flows (circulates) through the feed tubes.

15 The equation of state for hydrogen is given by the ideal gas law.

16 Axial end effects have negligible impact on the performance of the storage system.

Model Length Scales

The length scales of the storage system, listed in Table 1, were calculated with the geometry scoping model described in Hardy and Anton [1].

Table 1
Input to the Geometry Scoping Model

Parameter	Value
Mass of recoverable H_2 to be stored in vessel	1000.00 g
Practical ratio of moles H_2 to moles $NaAlH_4$ that can be stored in 12 minutes	1.5
Bulk density of $NaAlH_4$ powder	0.72 g/ cm^3
Hydride bed diameter, no walls	23.00 cm
Concentration of $NaAlH_4$ at the bed density	13,333.33 mole/m^3
Diameter of coolant tubes	1.91 cm
Diameter of H_2 injection tubes	1.27 cm
Number of coolant tubes	9

Number of H_2 injection tubes	8
Thickness of fin plates	0.0313 cm
Spacing between fin plates	0.63 cm
Tube wall thickness	0.12 cm
Density of tube material (6061-T6 Al from table on pg 6-11 of Avallone and Baumeister [35])	2.70 g/ cm^3
Density of fin material (6061-T6 Al from table on pg 6-11 of Avallone and Baumeister [35])	2.70 g/ cm^3
Material density of porous insert for H_2 delivery (6061-T6 Al from table on pg 6-11 of Avallone and Baumeister [35])	2.70 g/ cm^3

Heat Removal Parameters

Typical coolant flow velocities, convection heat transfer coefficients, pressure drops over the length of the coolant channels and the change in coolant temperature over the length of the coolant channels were estimated with the system heat transfer scoping model described in Hardy and Anton [1]. The coolant used in the model was Dowtherm T®, see Attachment 1 of Hardy [36], and the parameters calculated by the heat transfer scoping model are listed in Table 2.

Table 2.
Parameters From Heat Removal Scoping Model

Parameter	Value
Convection Heat Transfer Coefficient by Diitus-Boelter Correlation, Ref Holman [37]	0.4922 W/(cm^2 °C)
Coolant Mass Flux, Per Tube	1030.04 g/(cm^2 s)
Coolant Velocity	1260.73 cm/s
Re_D	56861.02
Pressure Drop Over Length of Coolant Tube	1.18E+01 psi
Bulk Coolant Temperature Increase Over Length of Coolant Tube	2.42 °C

Governing Equations and Boundary Conditions[1]

Hydrogen Mass Balance

The mass (mole) balance for hydrogen flowing through the bed is given by

$$\frac{\partial C_{nd}}{\partial t} + \nabla \cdot \left(C_{nd} \vec{v} \right) = \frac{1}{C_{ref}} \left(\frac{S_{H_2}}{\varepsilon} \right) \tag{1}$$

In a sodium alanate bed the uptake/discharge of hydrogen occurs via a two-step reaction given by

$$\underbrace{NaAlH_4}_{\text{Species 1}} \underbrace{\leftrightarrow}_{\text{Reaction 1}} \underbrace{\frac{1}{3} Na_3AlH_6}_{\text{Species 2}} + \frac{2}{3} Al + H_2 \underbrace{\leftrightarrow}_{\text{Reaction 2}} \underbrace{NaH}_{\text{Species 3}} + Al + \frac{3}{2} H_2 \tag{2}$$

The source rate for hydrogen is then

$$S_{H_2} = \left. \frac{\nu_{H_2}}{\nu_{NaH}} \right|_{Rxn2} \frac{\partial C_{NaH}}{\partial t} - \left. \frac{\nu_{H_2}}{\nu_{NaAlH_4}} \right|_{Rxn1} \frac{\partial C_{NaAlH_4}}{\partial t} \tag{3}$$

---

[1] Detailed derivations of all equations used in the model are presented in Appendix A.1 of Hardy [33].

Mass balance boundary conditions applied to the model are:

$$\left(C_{nd}\vec{v}\right)\cdot\hat{n} = 0 \quad \text{(on all walls and surfaces of symmetry)} \tag{4a}$$

and

$$C_{nd} = \frac{P_{inj}T_{ref}}{P_{ref}T_{wall}} \quad \text{(where the } H_2 \text{ feed tube wall joins the bed)} \tag{4b}$$

Hydrogen Velocities

The components of the hydrogen velocity are obtained from the Blake-Kozeny equation, see Bird, Stewart and Lightfoot [38]. Modifying the Blake-Kozeny equation to give the mean interstitial velocity, rather than the superficial velocity, gives the non-dimensionalized gas velocities

$$\begin{aligned} u_{nd} &= -\frac{D_p^{\,2}}{150\mu}\left(\frac{\varepsilon}{1-\varepsilon}\right)^2 \frac{P_{ref}}{U_{ref}}\frac{\partial P_{nd}}{\partial x} \\ v_{nd} &= -\frac{D_p^{\,2}}{150\mu}\left(\frac{\varepsilon}{1-\varepsilon}\right)^2 \frac{P_{ref}}{U_{ref}}\frac{\partial P_{nd}}{\partial y} \\ w_{nd} &= -\frac{D_p^{\,2}}{150\mu}\left(\frac{\varepsilon}{1-\varepsilon}\right)^2 \frac{P_{ref}}{U_{ref}}\frac{\partial P_{nd}}{\partial z} \end{aligned} \tag{5}$$

Bed Energy Balance

It is assumed that, at a given location, both the hydrogen contained within the voids of the bed, and the solid material comprising the bed, have the same instantaneous temperature. Thus, in the sense of temperature, the solid and gas phases of the bed are assumed homogeneous. Because hydrogen flows through the bed, it transports thermal energy by convection. The enthalpies of reaction occurring during the uptake and release of hydrogen constitute a heat source that is assumed to be uniformly distributed over the volume occupied by the bed. The bed energy balance treats both the solid and gas phases as a homogeneous region, and is given by

$$\rho_{bed} C_{p\ bed} \frac{\partial T_{nd}}{\partial t} - \nabla \cdot k \nabla T_{nd} = -\varepsilon \rho_{H_2} C_{p\ H_2} \left(\frac{\partial T_{nd}}{\partial t} + \vec{v} \cdot \nabla T_{nd} \right) + \frac{1}{T_{ref}} \left(\frac{\partial P}{\partial t} + \varepsilon \vec{v} \cdot \nabla P \right) + \frac{1}{T_{ref}} \text{Source} \tag{6}$$

The boundary conditions for the energy balance are:

$\hat{n} \cdot \nabla \cdot \left(k \nabla T_{nd} \right) = 0$ (thermal insulation, on all exterior boundaries and surfaces of symmetry) (6a)

$$\hat{n} \cdot \nabla \cdot \left(k \nabla T_{nd} \right) = -h_{H_2\ cool} \left(\frac{T_{wall} - T_{H_2\ bulk}}{T_{Ref}} \right) \quad \text{(on the walls of the } H_2 \text{ feed tubes)} \tag{6b}$$

Energy Balance for the Tubes and Fins

The energy balance within the metal composing the fins and tubes is

$$k_{metal}\nabla^2 T = \rho_{metal} C_{p\,metal}\frac{\partial T}{\partial t} \tag{7}$$

The boundary conditions applied to the metal tube and fins are:

$$\nabla\cdot\left(k_{metal\ 1}\nabla T_{metal\ 1}\right) = \nabla\cdot\left(k_{metal\ 2}\nabla T_{metal\ 2}\right) \quad \text{(at the interfaces between the fins and tubes)} \tag{7a}$$

$$\nabla\cdot\left(k_{metal}\nabla T_{metal}\right) = \nabla\cdot\left(k_{bed}\nabla T_{bed}\right) \quad \text{(at the interface between the bed and the metal)} \tag{7b}$$

$$\hat{n}\cdot\nabla\cdot\left(k_{metal}\nabla T_{metal}\right) = -h_{conv\ cool}\left(T_{wall} - T_{coolant\ bulk}\right) \quad \text{(on the walls of the cooling tubes)} \tag{7c}$$

Reaction Kinetics

Chemical kinetics depend on the material used as a storage media. Thus, to permit the kinetics equations to be easily modified, they are cast as a separate module within the set of governing equations defined in COMSOL Multiphysics® [34]. At present, the model can accept kinetics models in the form of differential-algebraic equations or as tabulated data (which can be fit using a cubic spline).

Reaction kinetics are based on the empirical kinetics model developed by the United Technologies Research Center™ (UTRC™), see Attachments 3 and 4, of [33]. The kinetics equations in the detailed model are identical to those used in the kinetics scoping model and were presented in Part 1 of this series of papers, Hardy and Anton [1].

The weight fraction of H_2 contained in the sodium alanate metal, based on Equation 2, is defined as

$$\begin{aligned} \text{wf} &= \frac{\text{Mass of recoverable } H_2 \text{ contained in the metal hydride at time t (kg } H_2)}{\text{Mass of the bed fully converted to tetrahydride form (kg } NaAlH_4)} \\ &= \frac{1.5C_1 + 0.5C_2}{C_{eqv}} \frac{M_{H_2}}{M_{NaAlH_4}} \end{aligned} \tag{8}$$

For sodium alanate, the reaction enthalpy term for the energy balance, Equation 6, is

$$\text{Source} = \frac{dC_1}{dt}\Delta H_{rxn\ 1} - 0.5\frac{dC_3}{dt}\Delta H_{rxn\ 2} \tag{9}$$

Equation of State

Over the range of operating temperatures and pressures for the storage system, hydrogen behaves as an ideal gas. Hence, the ideal gas law, in the form of Equation 10, constitutes the equation of state for the gas phase.

$$P = CRT \tag{10}$$

Model Input Parameters

Constant values and expressions used in the model are tabulated in Hardy [33]

Thermal Boundary and Initial Conditions for the Detailed Model

Temperatures and flowrates for the heat removal system were taken from Table 2. Given the small rise in the temperature of the heat transfer fluid over the length of the coolant tube, its temperature was assumed constant at 373K. The areal average velocity in the coolant tube was rounded to 13m/s.

The initial bed temperature was assumed to be 373K. Initially the hydrogen pressure in the tubes and the bed was 1 bar. The bed was initially pure NaH, with the stoichiometric quantity of Al required to complete the reaction to $NaAlH_4$. To effect charging of the media, the hydrogen pressure in the injection tubes was exponentially increased to 50 bar, reaching 99% of the final value in 10 seconds. As the gas pressure increased, the resulting pressure gradient caused the gas to flow from the tube and into the bed, according to the Blake-Kozeny equations. The hydrogen temperature in the injection tubes was fixed at 373K.

The bed length scales of both the 2 and 3-dimensional models were obtained from the geometry scoping model under the assumption that the hydride incorporated 1000 g of H_2, by complete conversion from NaH to $NaAlH_4$ in 12 minutes. As discussed in Hardy and Anton [1], the actual hydrogen loading is much lower than this value.

RESULTS

Transient calculations were performed for the charging phase of the sodium alanate bed. Although the state of the bed was conducive to loading, the kinetics equations used in the model were capable of modeling forward and reverse reactions, respectively implying charging and discharging of hydrogen. Based on the UTRC reaction kinetics model, described in [1], reaction 1 of Equation 2 reverses for $P_{eq1}(T)>P$ and reaction 2 of Equation 2 reverses for $P_{eq2}(T)>P$. Because $P_{eq1}(T)>P_{eq2}(T)$, reaction 1 reverses before reaction 2, and so reaction 1 may reverse while reaction 2 still goes forward.

The detailed models simultaneously solved the mass balance, energy balance, hydrogen velocity, chemical kinetics and other ancillary equations subject to the initial and boundary conditions. During the hydrogen charging process the penetration of hydrogen into the bed was driven by an increase in gas pressure in the hydrogen injection tubes, which was asymptotically increased from 1 to 50 bar, rising to within 99% of 50 bar in 10 seconds. The porous interface between the injection tube and the hydride bed allowed hydrogen to flow into the bed, which was initially at a pressure of 1 bar. As the pressure in the injection tube increased, the resulting pressure gradient within the packed hydride bed resulted in gas flow, which experienced viscous resistance as it passed into the bed. Uptake of hydrogen by the media affected both the pressure gradient and the mass flux. Heat generated by the chemical reactions was transferred to the cooling and gas injection tubes by conduction and to much lesser extent by forced convection as the gas flowed

through the bed. In the 3-dimensional model there was also heat conduction to the axially spaced fins. Of course, this effect was not treated in the 2-dimensional model.

Initial bed temperatures, coolant and gas temperatures in the 2 and 3-dimensional models were chosen to optimize the uptake kinetics. It was attempted to select temperatures that were sufficiently high to provide the most rapid uptake reaction rate, but not so high that exothermic reactions would yield bed temperatures that reversed the hydriding reaction.

Loading Rate

A comparison of loading rates for the 0-dimensional kinetics scoping model, and the 2 and 3-dimensional finite element models, in terms of the weight fraction of stored hydrogen, is shown in Figure 3. For the 0-dimensional kinetics scoping model, the weight fraction of stored hydrogen was point dependent, however, for the 2 and 3-dimensional finite element models, the weight fraction of stored hydrogen depended on location and time. Therefore, for the 2 and 3-dimensional models, the weight fraction of stored hydrogen was expressed as an areal or volume average, respectively. To demonstrate capability, the 2 and 3-dimensional finite element models were run for initial NaH concentrations of approximately 331 and 13,333 mole/m^3. Increasing the initial NaH concentration resulted in increase transient temperatures, which impacted the rate of hydrogen uptake.

Loading rates predicted by 3-dimensional finite element models, which allowed for axial heat transfer to the fins, were essentially identical to those for the 0-dimensional kinetics

model. The higher loading rates for the 2-dimensional (radial and azimuthal) finite element model, with an initial NaH concentration of 331 mole/m^3, resulted from higher bed temperatures due to the absence of fins. However, for the larger initial NaH concentration of 13,333 mole/m^3, temperatures in the 2-dimensional model were sufficiently high to reduce and in some locations reverse reaction 1 of the hydriding reactions, see Equation 2. This led to a lower loading rate as shown in Figure 3.

Three models were used to estimate the hydrogen charging rate for the bed. These were the kinetics scoping model and the detailed 2 and 3-dimensional finite element models. The kinetics scoping model determined charging rate by solving the kinetics equations for a fixed temperature of 373K and a fixed hydrogen pressure of 50 bar.

Bed Temperatures

Heat generated during the loading of the bed results in a temperature transient that impacts the reaction rates. The low thermal conductivity of the alanate necessitates design features that maintain a relatively short length scale for heat transfer within the bed. The models in this document were developed for shell and tube (the 2-dimensional finite element model) and shell, tube and fin (the 3-dimensional finite element model) configurations.

Figure 4 shows plan and isometric views of the temperature profile in the 3-dimensional model at 40 seconds into the charging transient. The image on the left shows the

reduction in temperature from the mid-plane of the hydride layer to the midplane of the fin. The plan view, on the right, shows the temperature profile over the midplane of the hydride layer.

Figures 5 through 7 compare the transient temperature profile for the 2-dimensional model, which does not have fins, to the temperature profile at the midplane of the hydride layer for the 3-dimensional model. Comparisons were made at 30, 120 and 720 seconds. As expected, these figures show that heat transfer to the fins results in a much more uniform temperature profile.

Bed Gas Flow

The relation between the pressure gradient and the gas velocity is represented by the Blake-Kozeny equation. By this equation, the small effective diameter of the particles comprising the bed results in significant resistance to flow. As the local gas pressure in the bed increases, hydrogen is removed from the gas phase as the hydriding reactions take place. Heating of the gas by the exothermic reactions, in turn, affects the gas pressure and the reaction rates. Expansion work performed as the gas flows opposite the direction of the pressure gradient also has an effect, although slight, on the gas temperature. These complex, coupled phenomena are considered in the energy, continuity and kinetics equations.

Figures 8 and 9 show the magnitude and direction of the hydrogen velocity for the 2 and 3-dimensional finite element models at times of 10 and 40 seconds, respectively.

Hydride Concentration Profiles

Conversion of NaH to Na_3AlH_6 and then to $NaAlH_4$ occurs as the bed is loaded with hydrogen. However, the formation of hexa and tetra-hydrides is most rapid in locations that have temperatures and pressures conducive to higher reaction rates. To use the bed efficiently, the concentration of tetra-hydride must be relatively uniform at the termination of the loading phase. Optimizing hydrogen loading rates and achieving full utilization of the bed requires design features that ensure proper heat transfer and flow.

Figures 10 through 12 compare the transient concentrations of Na_3AlH_6 and $NaAlH_4$ for the 2-dimensional model and at the midplane of the hydride for the 3-dimensional model.

CONCLUSIONS

A general methodology was developed for detailed performance modeling of a media based hydrogen storage system. In this paper the detailed models were applied to a storage vessel having the form of a modified shell and tube heat exchanger, with fins normal to the axis. The storage media used in this system was $TiCl_3$ catalyzed $NaAlH_4$. The detailed 2 and 3-dimensional storage system models calculate time and spatially dependent pressure, temperature, molar concentrations of $NaAlH_4$, Na_3AlH_6, and NaH, the three components of gas velocity, gas concentration and/or density. In addition, the models can compute algebraic combinations, integrals and time or spatial derivatives of the above variables. The ability to manipulate dependent variables is essential for sensitivity studies that identify those parameters having the most significant impact on

storage system performance. As improved types of storage media are discovered and storage system concepts evolve, new calculations and sensitivity studies will be required. Until more concrete information is available, however, the exact nature of these computations is unknown. The generality of the detailed models, and the entire hierarchical modeling system, allows it to be applied as data becomes available.

It was found that the modified shell and tube heat exchanger was very effective from the perspective of heat removal and temperature control, permitting far better control of the bed temperature than the system without fins. This was clearly demonstrated by comparing the temperatures predicted by the 3-dimensional and 2-dimensional models, which represented storage systems with and without fins, respectively, see Figures 5 through 7. At higher concentrations of the storage media, the superior temperature control for the modified heat exchanger allowed loading rates to be maximized. As seen from Figure 3, the charging rate for the finned system is essentially the same as that predicted by the 0-dimensional kinetics scoping model. This means that charging in the finned system is limited by kinetics alone, which represents an upper bound to the charging rate at a given temperature and pressure. The more uniform spatial temperatures in the modified storage system yielded smaller spatial concentration gradients for the hexa and tetra-hydrides formed from NaH, resulting in more efficient utilization of the bed. The effect on the spatial concentrations of the hydrides for the two types of heat exchangers is shown in Figure 12.

SUMMARY

As presented in Hardy and Anton [1], and this paper, the hierarchical methodology for evaluation of hydrogen storage systems consists of four sub-models:

- A 0-dimensional kinetics scoping model that evaluates loading and discharge kinetics, along with the maximum storage capacity, for a given hydride.
- A geometry scoping model which determines system length scales required to store a given amount of hydrogen for a particular hydride and geometric configuration. The model also calculates placement of heat transfer elements, and the gravimetric and volumetric capacities for the system.
- A scoping model that estimates coolant flowrates, temperatures, pressure drops, etc., required to remove heat generated during hydrogen uptake. This model can also be used to identify suitable heat transfer fluids.
- Finite element models in 2 and 3-dimensions that couple mass, momentum and heat transfer, along with pressure and temperature dependent chemical kinetics. These models are used to evaluate the detailed performance of the storage system.

The hierarchical models are sequentially applied as follows:

1 The hydride kinetics are evaluated with the 0-dimensional kinetics scoping model. The model is used to determine the dependence of the reaction rates and hydrogen capacity on temperature and pressure. Pressures and temperatures that optimize loading and discharge rates are determined and possible errors in the kinetics model are identified. The bed gravimetric

and volumetric capacities are calculated from the loading calculations and the bulk density of the storage material.

2 The hydrogen weight fraction from the kinetics scoping model, component densities, component length scales and the required mass of hydrogen to be stored are input to the geometry scoping model. The model calculates the size of the system, the location of heat transfer elements, as well as the gravimetric and volumetric capacities of the system.

3 System length scales from the geometry scoping model, heat transfer fluid properties, thermal properties of the system components, heats of reaction, total amount of hydrogen to be stored and the time required to load the system are input to the heat transfer scoping model. The model calculates the coolant flowrates, convection heat transfer coefficients and other parameters required to remove heat generated by the chemical reactions governing hydrogen uptake. The model is useful for determining whether the operating parameters required for the cooling system are attainable and/or practical.

4 The storage vessel length scales, geometry, heat transfer parameters and bed configuration are input to the 2 and/or 3-dimensional detailed models. A number of other input parameters including material properties, flowrates, reaction kinetics, etc. are also required.

5 The detailed models are used to assess the ability of the system to meet technical requirements.

6 System design is refined by repeating steps 1 through 5 with modified parameters.

ACKNOWLEDGEMENTS

This document was prepared in conjunction with work accomplished under Contract No. DE-AC09-08SR22470 with the U.S. Department of Energy.

DISCLAIMER

REFERENCES

[1] Hardy BJ, Anton DL. Hierarchical modeling system for hydrogen storage systems. Part I: scoping models. Int J Hydrogen Energy, in publication.

[2] Aldas K, Mat M. Numerical analysis of hydrogen storage in metal-hydride beds. Turk J Eng Environ Sci 2002;26:201-207.

[3] Aldas K, Mat M, Kaplan Y. A three-dimensional model for absorption of hydrogen in a metal hydride bed. Int J Hydrogen Energy 2002;10(27):1049-1056.

[4] Anton DL, Mosher DA. High density hydrogen storage system demonstration using $NaAlH_4$ complex compound hydride. Proceedings of the 2005 hydrogen program, 2005.

[5] Askri F, Jemni A, Nasrallah SB. Prediction of transient heat and mass transfer in a closed metal-hydrogen reactor. Int J Hydrogen Energy 2004;29:195-208.

[6] Bilgili M, Ataer ÖE. Numerical analysis of hydrogen absorption in a P/M bed. Powder Technology 2005;160:141-148.

[7] Botzung M, Chaudourne S, Gilla O, Perret C, Latroche M, Percheron-Guegan A, Marty P. Simulation and experimental validation of a hydrogen storage tank with metal hydrides. Int J Hydrogen Energy 2008;33(1):98-104.

[8] Brown TM, Brouwer J, Samuelsen GS, Holcomb FH, King J. Accurate simplified dynamic model of a metal hydride tank. Int J Hydrogen Energy 2008;33(20):5596-5605.

[9] El-Gammal MA, El-Osairy MA, El-Osery IA, Metwally AM, Hassan MA. A study for the major factors affecting the hydrogen discharging in the metal hydrogen storage conduction bed model. Modelling Measurement and Control 1993;2(46):35-44.

[10] El-Osairy MA, El-Osery IA, Metwally AM, Keshk MM. Temperature and composition analysis of a convective model of metal hydride hydrogen storage beds. Int J Hydrogen Energy 1992a; 2(17):125-128.

[11] El-Osairy MA, El-Osery IA, Metwally AM, Keshk MM. On the optimization of convective hydrogen storage bed model using $LaNi_5H_6$ or $FeTiH_{1.6}$. Int J Hydrogen Energy 1992b;17(17):961-964.

[12] El-Osairy MA, El-Osery IA, Metwally AM, Hassan MA. Temperature and composition distributions of $FeTiH_{1.6}$ and $MgNiH_4$ for two-dimensional hydrogen energy conduction bed model. J Alloys and Compounds 1993;202:125-128.

[13] El-Osairy MA, El-Osery IA, Metwally AM, and Hassan MA. Temperature and composition distributions of $LaNi_5H_6$ metal hydride for different geometries and flow regimes in hydrogen energy conduction bed model. Modelling Measurement and Control 1994;1(40):53-63.

[14] El-Osery IA. A comparative study of “in-out” and “out-in” hydrogen reaction alternatives for metal hydride beds using RET1 computer code. Int Assoc Hydrogen Energy 1984a;5(9):421-444.

[15] El-Osery IA. A comparative study of different designs for metal hydride hydrogen storage beds using TOBA computer code. Proceedings of hydrogen energy progress V, 5^{th} world hydrogen conference. Toronto; July 15-20 1984b. Volume 3, p. 1383-1392. Oxford: Pergamon Press.

[16] El-Osery IA. On computer calculations of temperature-composition relations in metal hydride hydrogen storage beds. Surface and Coatings Tech. 1986;28:397-404.

[17] El-Osery IA, El-Osairy MA, Metwally AM., Keshk MM. and El-Gammal MA. Dynamic simulation of the convective model for metal hydride hydrogen storage beds. Energy Sources 1993;(15):523-530.

[18] Gadre S, Ebner A, Al-Muhtaseb S, Ritter J. Practical modeling of metal hydride hydrogen storage systems. Ind Eng Chem. Res. 2003;(42):1713.

[19] Gopal MR, Murthy SS. Prediction of heat and mass transfer in annular cylindrical metal hydride beds. Int J Hydrogen Energy 1992;10(17):795-805.

[20] Gopal MR, Murthy SS. Studies on heat and mass transfer in metal hydride beds. Int J Hydrogen Energy 1995;11(20):911-917.

[21] Gross KJ. The reversible hydrides solution for hydrogen storage. G-CEP hydrogen workshop. Stanford, CA; April 14-15, 2003. Available from: http://gcep.stanford.edu/pdfs/hydrogen_workshop/Gross.pdf [accessed 3.12.08].

[22] Gross KJ, Majzoub E, Thomas GJ., and Sandrock G. Hydride development for hydrogen storage. Proceedings of the DOE hydrogen program 2002 annual merit review. Golden, CO; April 14-15, 2002. Available from: http://www1.eere.energy.gov/hydrogenandfuelcells/pdfs/32405b32.pdf [accessed 3.12.08].

[23] Ha MY, Kim IK, Song HD, Sung S, Lee DH. A numerical study of thermo-fluid phenomena in metal hydride beds in the hydriding process. Int J Heat and Mass Transfer 2004,(47):2901.

[24] Jemni A, Nasrallah SB. Study of two-dimensional heat and mass transfer during absorption in a metal-hydrogen reactor. Int J Hydrogen Energy 1995;1(20):43.

[25] Jemni A, Nasrallah, B, Lamloumi, J. Experimental and theoretical study of a metal-hydrogen reactor. Int J Hydrogen Energy 1999;(24):631.

[26] Kikkinides ES, Georgiadis MC, Stubos AK. Dynamic modeling and optimization of hydrogen storage in metal hydride beds. Energy 2006;31:2428.

[27] Lide DR, Kehiaian HV. CRC Handbook of thermophysical and thermochemical data. Boca Raton, FL: CRC Press, 1994.

[28] Mat M, Kaplan Y. Numerical study of hydrogen absorption in a $LaNi_5$ hydride reactor. Int J Hydrogen Energy 2001;9(26):957-963.

[29] Mayer U, Groll M, Supper W. Heat and mass transfer in metal hydride reaction beds experimental and theoretical results. J Less Common Met 1987;131:235-244.

[30] Mazumdar S, Gopal MR, Bhattacharyya S. Thermodynamic analysis and optimization of compressor-driven metal hydride cooling systems. Int J Hydrogen Energy 2005,(30):631.

[31] Mosher D, Tang X, Arsenault S, Laube B, Cao M, Brown R and Saitta S. High density hydrogen storage system demonstration using NaAlH4 complex

compound hydrides. Proceedings of the DOE hydrogen program 2007 annual merit review. Arlington, VA; May 15-18, 2007. Available from: http://www.hydrogen.energy.gov/pdfs/review07/stp_33_mosher.pdf [accessed 3.12.08].

[32] Nasrallah SB, Jemni A. Study of two-dimensional heat and mass transfer during desorption in a metal-hydrogen Reactor. Int J Hydrogen Energy 1997;1(22):67.

[33] Hardy BJ. Integrated hydrogen storage system model. Report, WSRC-TR-20007-00440, rev.0. Savannah River National Laboratory. Available from: http://www1.eere.energy.gov/hydrogenandfuelcells/pdfs/bruce_hardy_srnl-2007-0043_part2.pdf#h2_storage and http://sti.srs.gov/fulltext/WSRC-TR-2007-00440.pdf; November 16, 2007 [accessed 3.12.08].

[34] COMSOL Multiphysics®, version 3.3.0.405. Copyright 1994-2006, COMSOL AB.

[35] Avallone EA, and Baumeister III T. Mark's standard handbook for mechanical engineers, 9th edition. New York, NY: McGraw-Hill, 1987.

[36] Hardy BJ. Geometry, heat removal and kinetics scoping models for hydrogen storage systems. Report WSRC-TR-2007-00439, rev. 0. Savannah River National Laboratory. Available from: http://www1.eere.energy.gov/hydrogenandfuelcells/pdfs/bruce_hardy_srnl-2007-0043_part1.pdf and http://sti.srs.gov/fulltext/WSRC-TR-2007-00439.pdf ; November 16, 2007 [accessed 3.12.08].

[37] Holman JR. Heat transfer, 4th edition. New York, NY: McGraw-Hill, 1976.

[38] Bird RB, Stewart WE, Lightfoot EN. Transport phenomena. New York, NY: John Wiley & Sons, 1960.

FIGURES

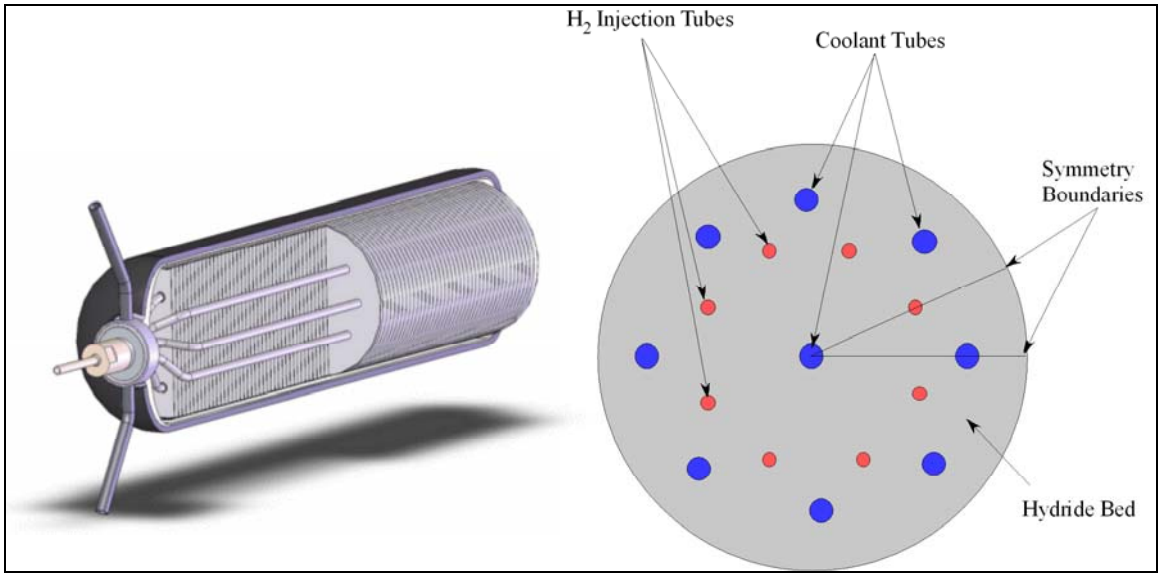

Figure 1. The illustration to the left is a shell, tube and fin hydride bed configuration, Mosher, et. al. [31]. The illustration to the right is a cross-section of the hydride bed used in the detailed model.

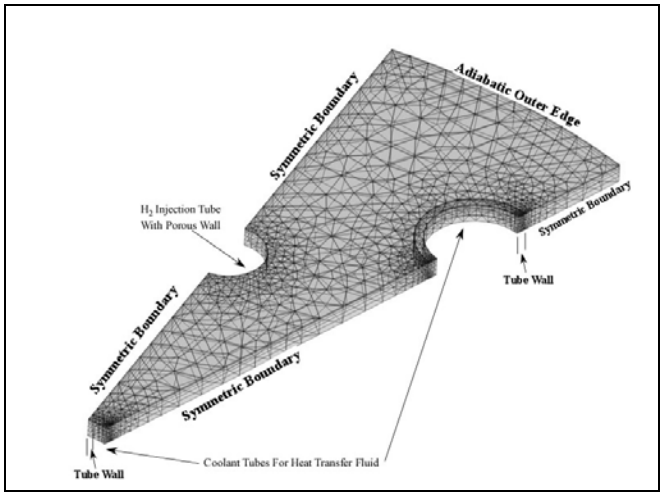

Figure 2. Geometry used for computations in the 3-dimensional model. The geometry for the 2-dimensional model is the planar form of that in the figure.

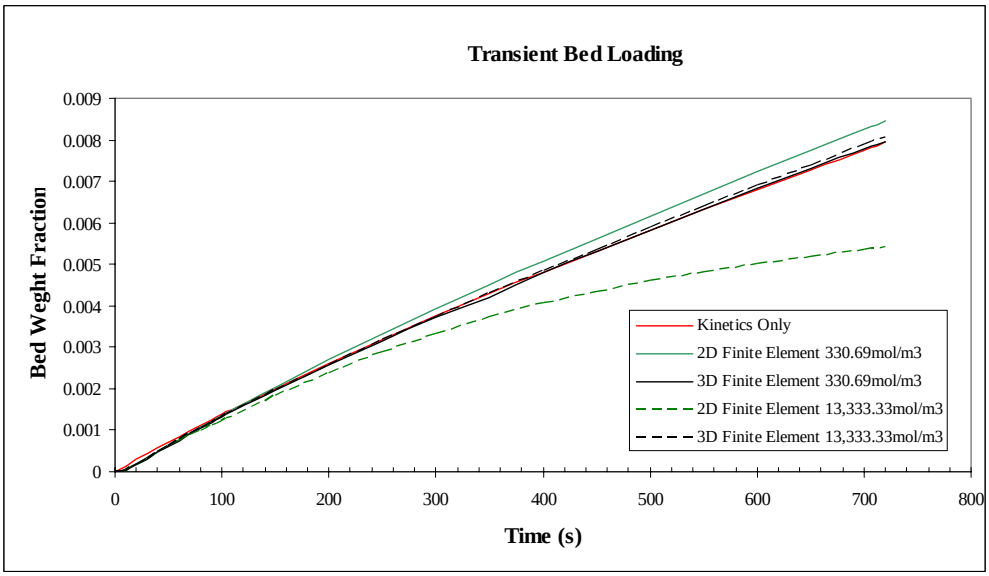

Figure 3. Comparison of the weight fraction of stored hydrogen for the kinetics scoping model and the 2 and 3-dimensional finite element bed models.

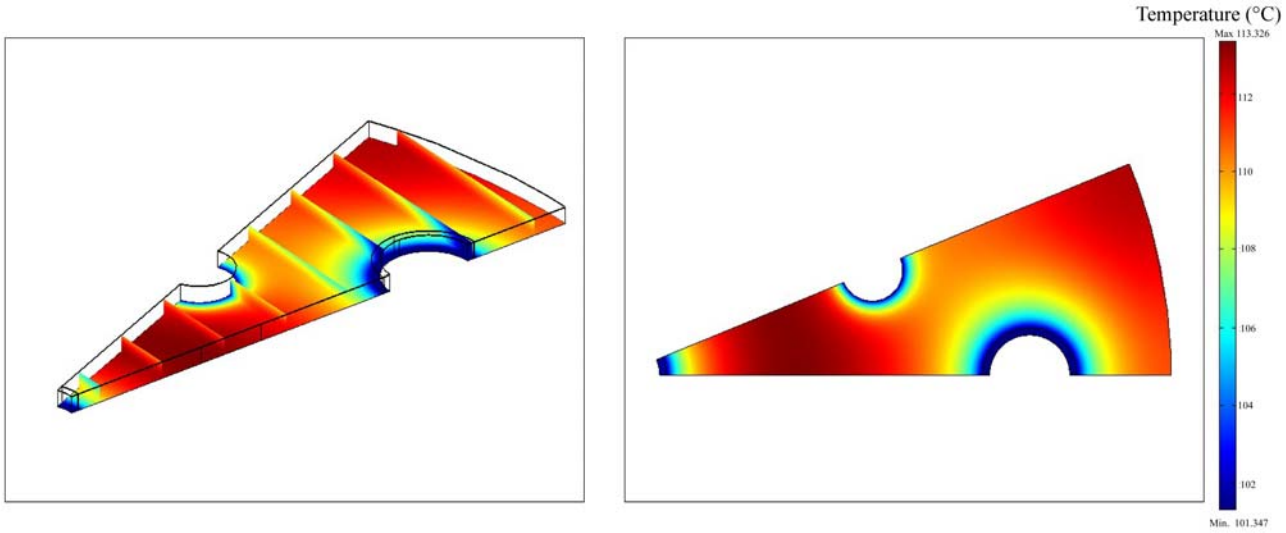

Figure 4. Isometric and plan views of temperature profile for 3-dimensional model at 40 seconds. Base of isometric figure is at bed midplane (center of the hydride bed layer between fins).

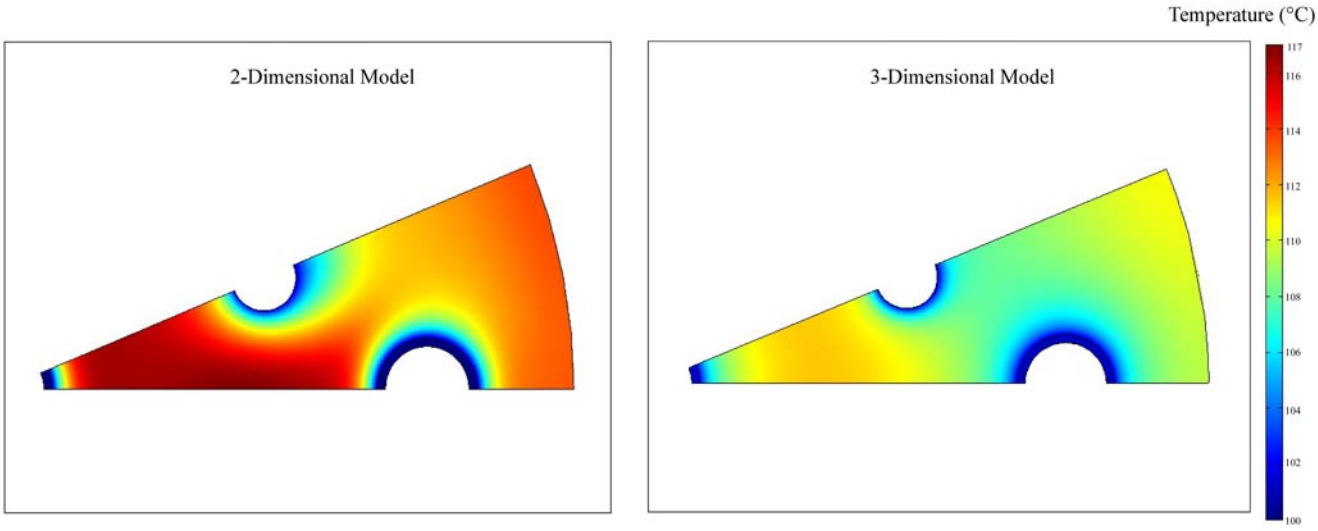

Figure 5. Comparison between 2-dimensional and 3-dimensional bed midplane temperature profiles at 30 seconds.

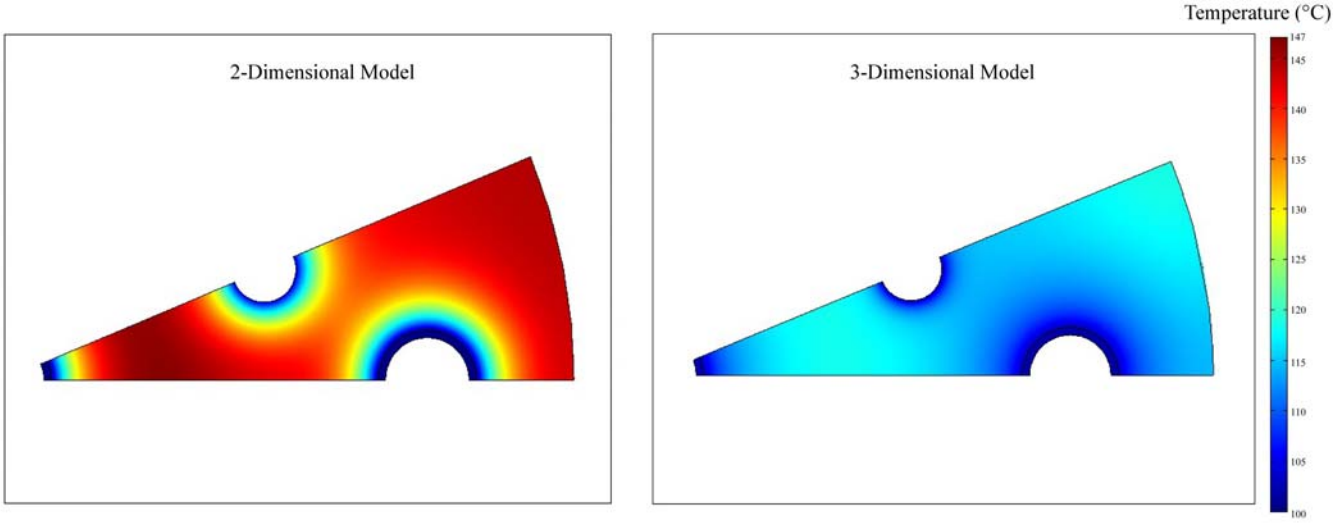

Figure 6. Comparison between 2-dimensional and 3-dimensional bed midplane temperature profiles at 120 seconds.

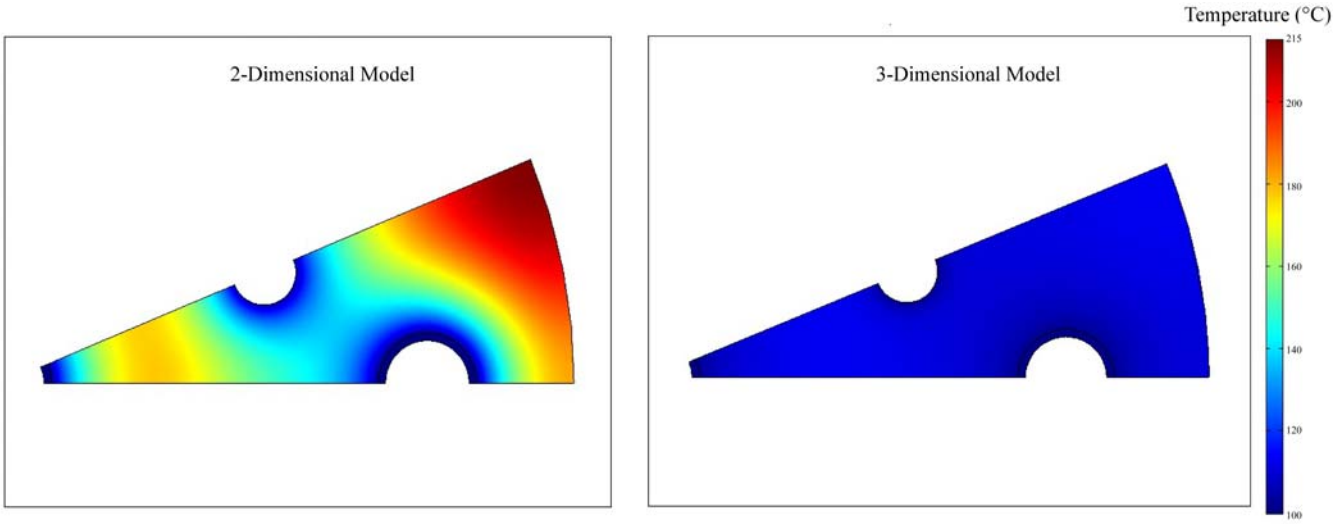

Figure 7. Comparison between 2-dimensional and 3-dimensional bed midplane temperature profiles at 720 seconds.

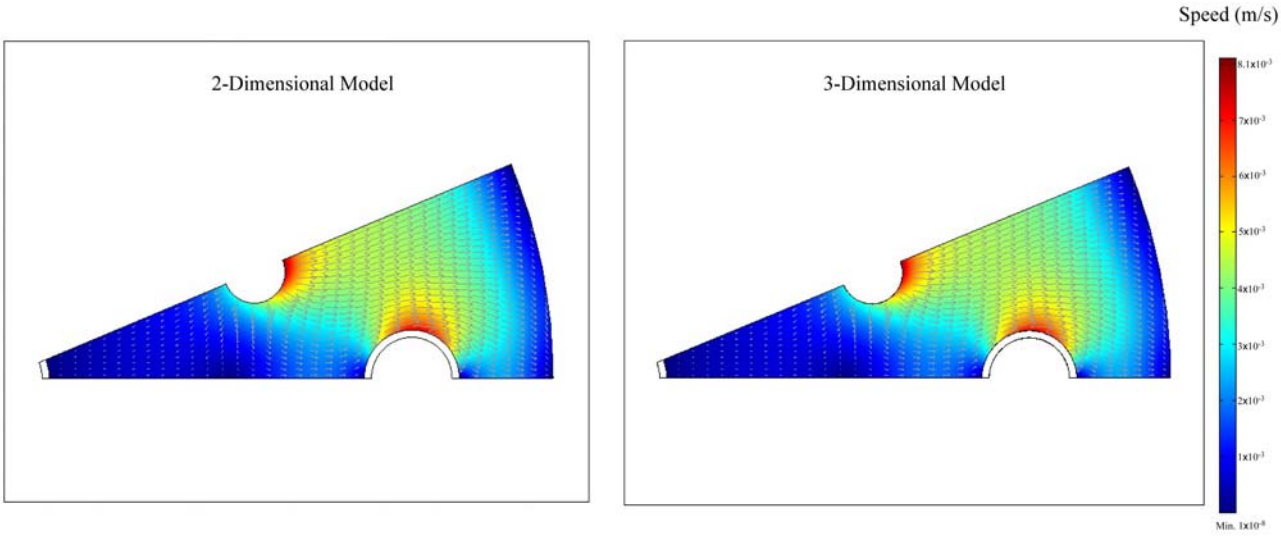

Figure 8. Hydrogen velocity profile across bed midplane at 10 seconds.

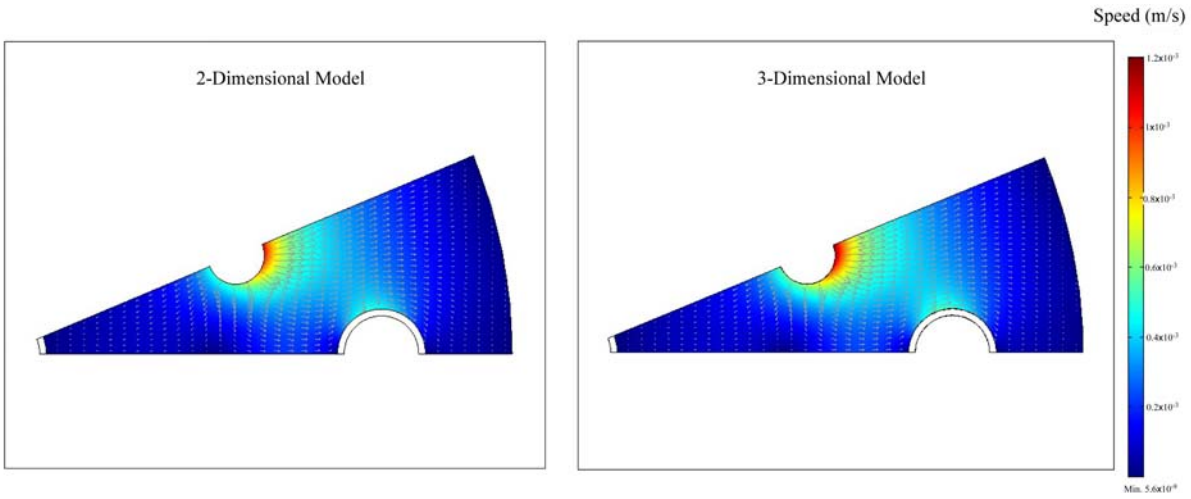

Figure 9. Hydrogen velocity profile across bed midplane at 40 seconds.

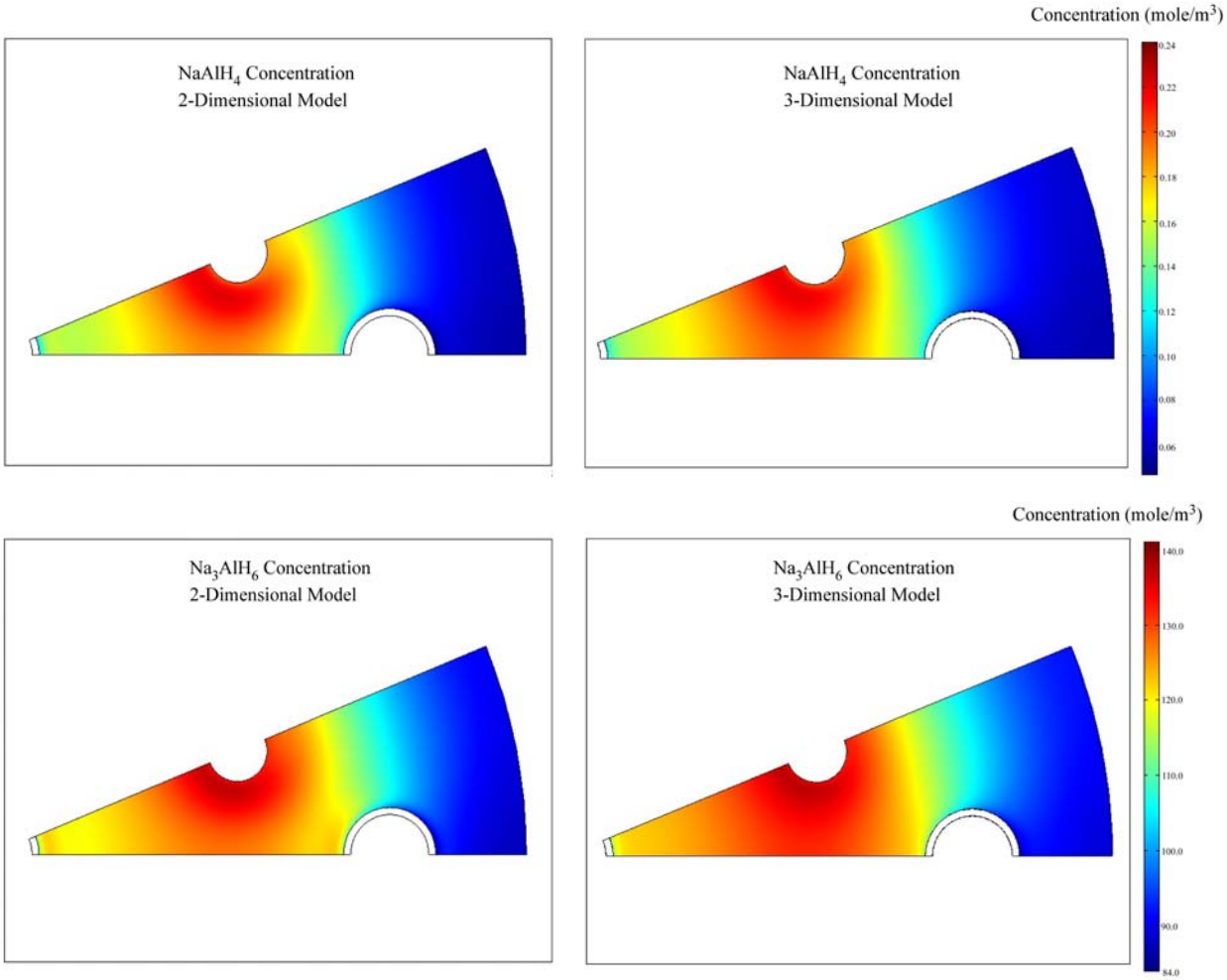

Figure 10. Comparison of 2-dimensional and 3-dimensional bed midplane hydride concentrations at 40 seconds.

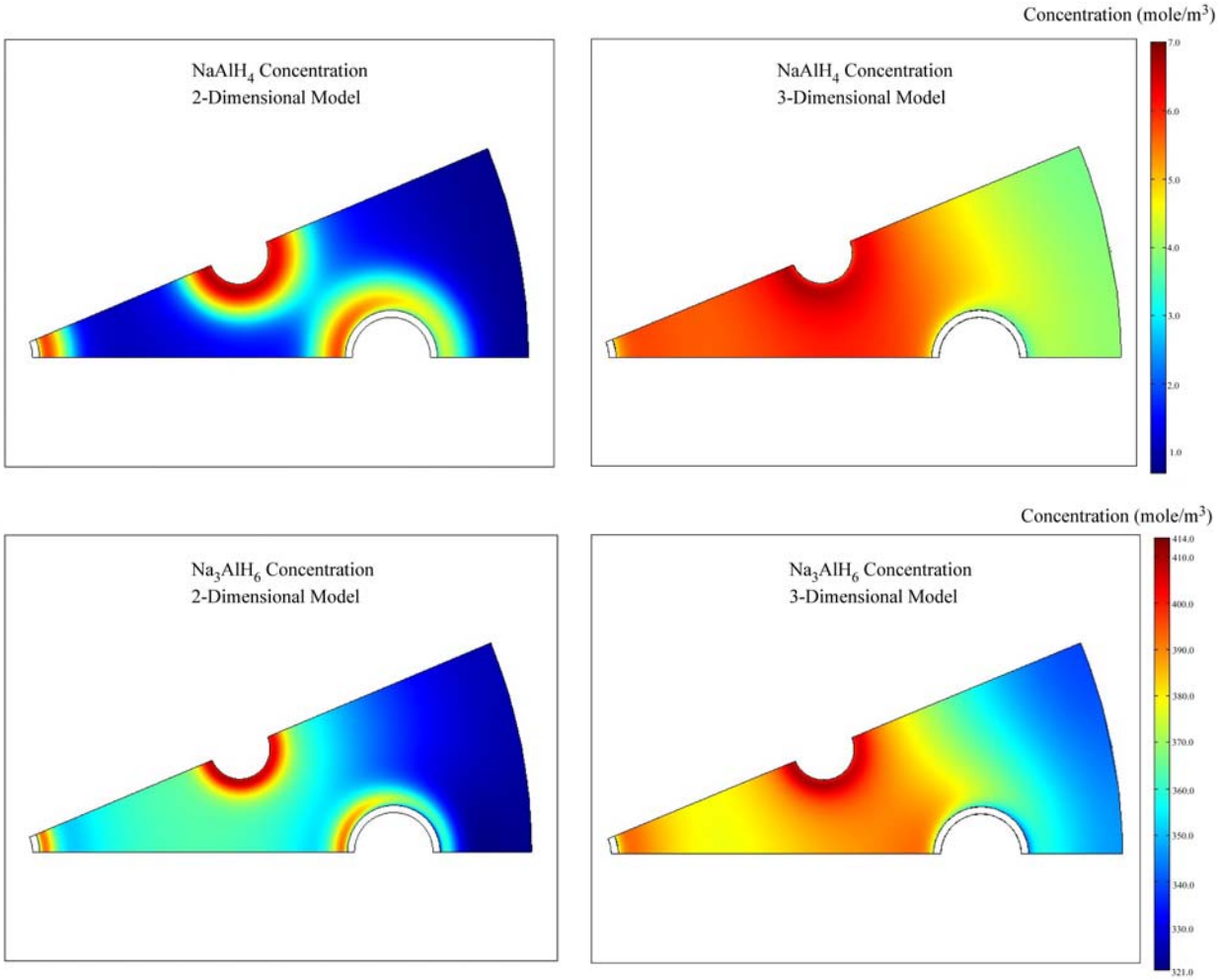

Figure 11. Comparison of 2-dimensional and 3-dimensional bed midplane hydride concentrations at 120 seconds.

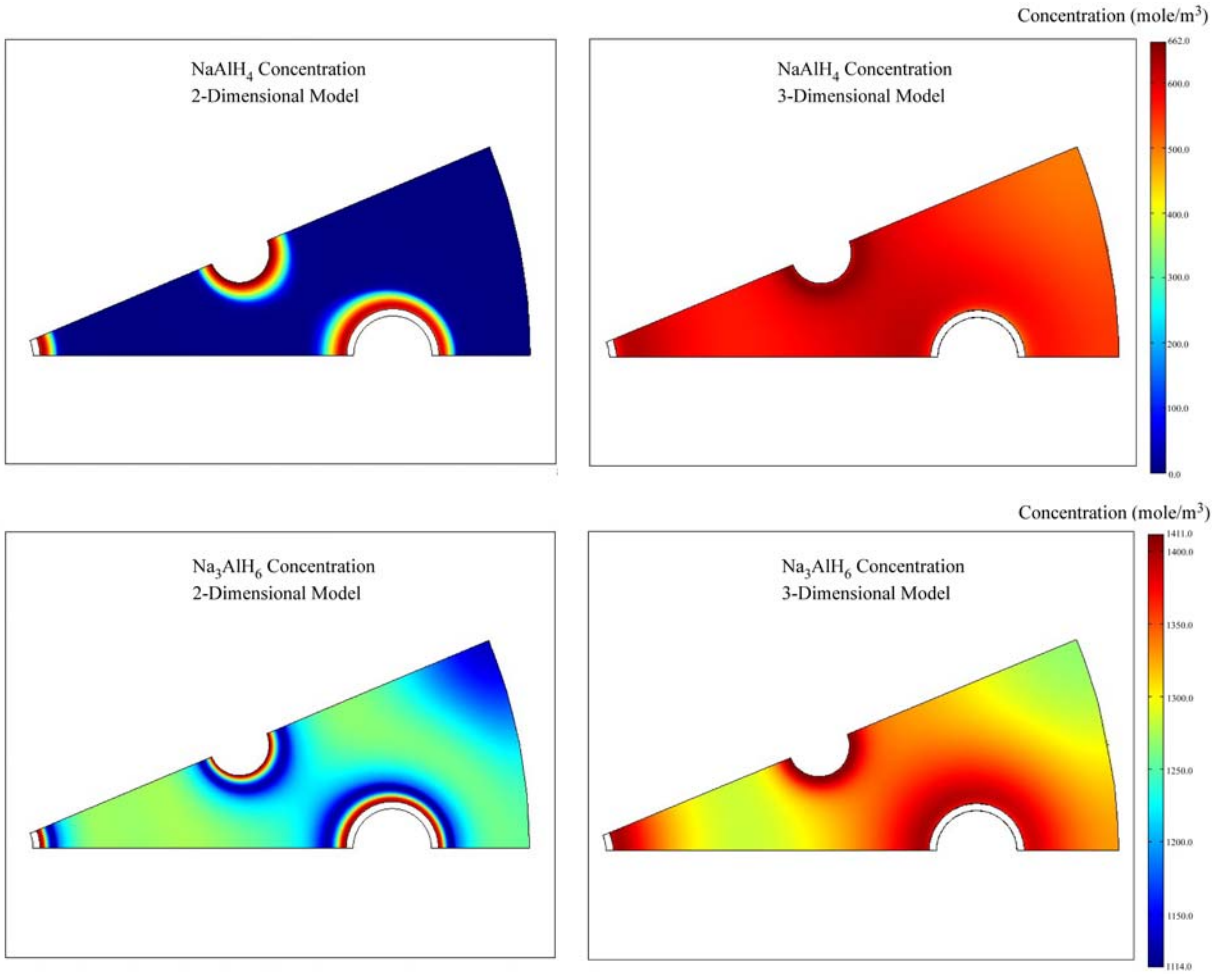

Figure12. Comparison of 2-dimensional (without fins) and 3-dimensional (with fins) bed midplane hydride concentrations at 720 seconds.